Tuning interfacial electronic properties of palladium oxide on vacancy-abundant carbon nitride for low-temperature dehydrogenation

Hao Chen,[1] Huili Shuang,[1] Wenwen Lin,[1] Xiaoxuan Li[1], Zihao Zhang,[1] Jing Li,[1] Jie Fu*[1, 2]

[1] Key Laboratory of Biomass Chemical Engineering of Ministry of Education, College of Chemical and Biological Engineering, Zhejiang University, Hangzhou 310027, China.

[2] Institute of Zhejiang University-Quzhou, 78 Jiuhua Boulevard North, Quzhou 324000, China

E-mail: jiefu@zju.edu.cn

Experimental Section

Materials

N-ethylcarbazole and 2-methylindole were purchased from J&K (Beijing, China). Urea was purchased from Macklin. N-propyl-carbazole was purchased from Ark Pharm (Arlington Heights, USA). Palladium on activated carbon (Pd/AC, 5 wt%) and ruthenium on carbon (Ru/AC, 5 wt%) were purchased from Sigma Aldrich (St. Louis, USA). zirconyl chloride octahydrate, sodium tetrachloropalladate (II), sodium borohydride and monoclinic zirconia were purchased from Shanghai Aladdin Bio-Chem Technology.

Preparation of Zr-C_3N_4

Based on our previous study[1], 0.3g of zirconyl chloride octahydratea and 10 g urea were dissolved in 30 mL deionized water . The solution was evaporated to dryness after ultrasonic solution for one hour, and white crystal were obtained and loaded into a 30 mL crucible with a lib. Then, the crystals were calcined in a muffle furnace from 30 °C to 550 °C with a ramp rate of 2 °C/min and maintained at 200 °C for 1.5 h, and then further increased to 550 °C and maintained for 2 h. The resulting product was grinded to give a yellow powder named as Zr-C_3N_4.

Preparation of C_3N_4

10 g urea were loaded into a 30 mL crucible with a lib. Then, the crystals were calcined in a muffle furnace from 30 °C to 550 °C with a ramp rate of 2 °C/min and maintained for 2 h. The resulting product was grinded to give a yellow powder named as C_3N_4.

Preparation of PdO/Zr-C_3N_4, PdO/C_3N_4 and Pd^0/Zr-C_3N_4

PdO/Zr-C_3N_4, PdO/C_3N_4 and Pd^0/Zr-C_3N_4 (5 wt% Pd loading) were synthesized by liquid-phase reduction method. Sodium tetrachloropalladate(II) and Zr-C_3N_4 (or C_3N_4, t-ZrO_2) were solvent in 30 mL deionized water with stirring at room temperature for 1 h, then the fresh sodium tetrahydridoborate (2~10 equiv per Pd) dissolved in 4mL deionized water at 5 °C and was added dropwise to the solution with rapid stirring, leading to an instantaneous change of solution color from yellow to dark back. The solution was stirred for an additional 3 h, filtered, washed, dried and named Pd^0/C_3N_4 and Pd0/Zr-C_3N_4.

Then the Pd^0 based was dried at120 °C for36h and then calcined from 30 °C to 380 °C in a muffle furnace with a heating rate of 5 °C/min, keeping for 12 h. The catalysts were named as PdO/Zr-C_3N_4 (PdO/C_3N_4).

Preparation of Pd nanoparticles and supported catalysts

The Pd nanoparticles (NPs) was synthesized according to the reference. [2] Then the Pd NPs was loading on the C_3N_4 and Zr-C_3N_4. The catalysts were dried at120 °C for36h. Then, they were calcined from 30 °C to 380 °C in a muffle furnace with a heating rate of 5 °C/min, keeping for 12 h. The catalysts were named as PdO NPs/Zr-C_3N_4 (PdO NPs/C_3N_4).

Preparation of hydrogen-rich-LOHCs

0.24 g N-ethylcarbazole, 0.36 g N-propyl-carbazole, 0.4 g 2-methylindole and 0.1 g Ru/AC (5 wt% Ru loading) were loaded into 100 mL stainless steel batch reactor. Then, the ultrahigh purity hydrogen was added to reactor to 4 Mpa, and this pressurization process was repeated three times. The reactor was heated to 230 °C in an oil bath.

Characterization

Transmission electron microscopy (TEM) images were obtained using a JEOL-2100f. The Pd and Zr concentration in the catalysts were calculated by inductive coupled plasma optical emission spectrometry (ICP-OES) using a Varian T30-ES. The specific surface areas were calculated using the Brunauer–Emmett–Teller (BET) equation. The X-ray

photoelectron spectroscopy (XPS) were performed on Thermo Scientific K-Alpha. The X-ray diffraction (XRD) profiles of catalysts were obtained (X-pert Powder, the Netherlands) with a Rigaku D/max-III X-ray power diffractometer. The Electron Paramagnetic Resonance (EPR) of catalysts were performed on EMXmicro-6/1/P/L. The Cyclic Voltammetry (CV) and Electrochemical Impedance Spectroscopy (EIS) of catalysts were obtained on CHI660E. The hydrogenation temperature-programmed reduction (H_2-TPR) and CO chemisorption were performed using a Chemisorption Physisorption Analyzer (FINESORB-3010, FINETEC, China).

Catalytic dehydrogenation

0.25g of liquid hydrogen-rich LOHCs and catalyst were loaded in an 8 mL autoclave. The reactor was washed by nitrogen atmosphere three times and heated to required temperature for some hours, and then placed in water to cool to room temperature. The liquid was collected, diluted with acetone, analyzed by GC/FID (Agilent 7890B) and were confirmed by GC-MS (Agilent 5977A MSD). N_2 flow was using during the dehydrogenation to take away the H_2 produced and prevent the reduction of PdO.

The TOF of the series of catalyst was estimated based on the following equation, as reported in:

$$\text{TOF}\ (h^{-1}) = \frac{Amount\ of\ H-LOHC\ (\mu mol) \times yield\ of\ completely\ dehydrogenated\ products(\%)}{CO\ uptake\ \left(\frac{\mu mol}{g}\right) \times Amount\ of\ \text{catalyst}\ (g) \times Reaction\ time\ (h)}$$

During the dehydrogenation of 12H-NECZ, which is a heterogenous catalytic process, molecular diffusion in the liquid phase and surface adsorption are fast processes and the surface reactions dictate the overall reaction rates [3-4] Thus, people always assumed that the influence of internal and external diffusion can be neglected in the kinetic calculation of the reaction. And many other heterogeneous catalytic reactions were also the same as the dehydrogenation of 12H-NECZ [5-9]. Thus, in this work we also assumed that this system is kinetically controlled.

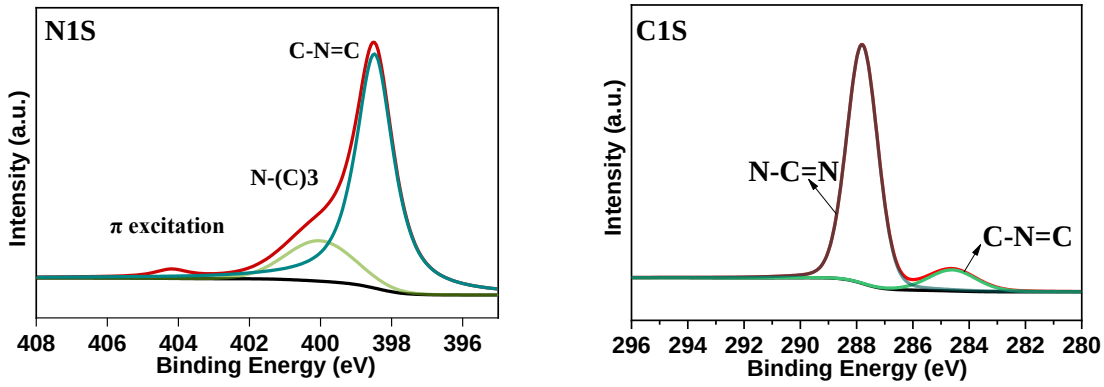

Figure S1. X-ray photoelectron spectroscopy (XPS) of C1s XPS spectra and N1s XPS spectra of Zr-C_3N_4.

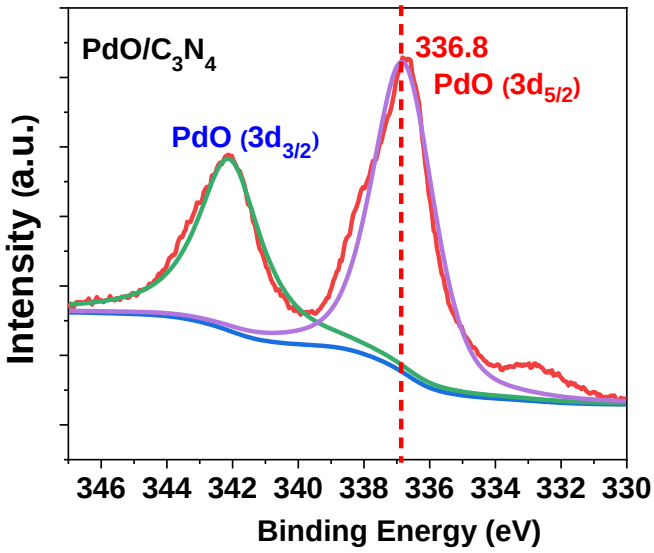

Figure S2. X-ray photoelectron spectroscopy (XPS) of PdO/C_3N_4.

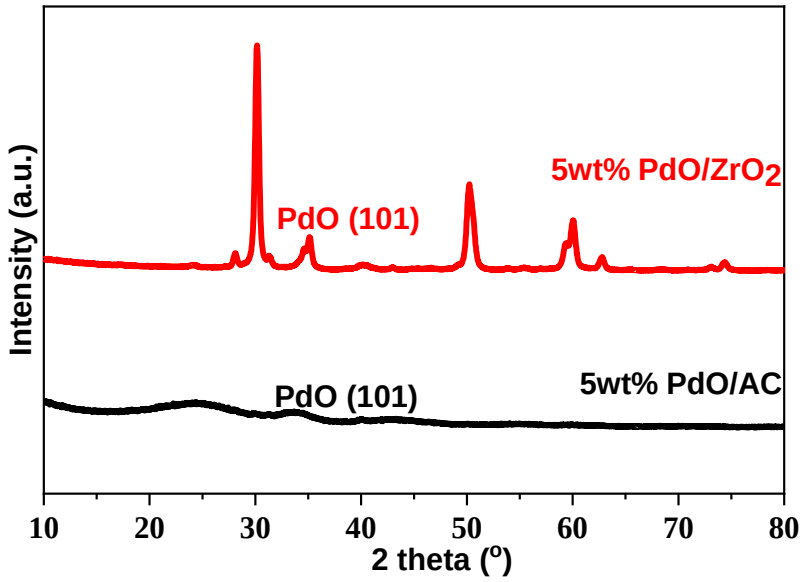

Figure S3. Powder X-ray diffraction patterns (XRD) patterns of PdO/AC, PdO/ZrO_2 catalysts.

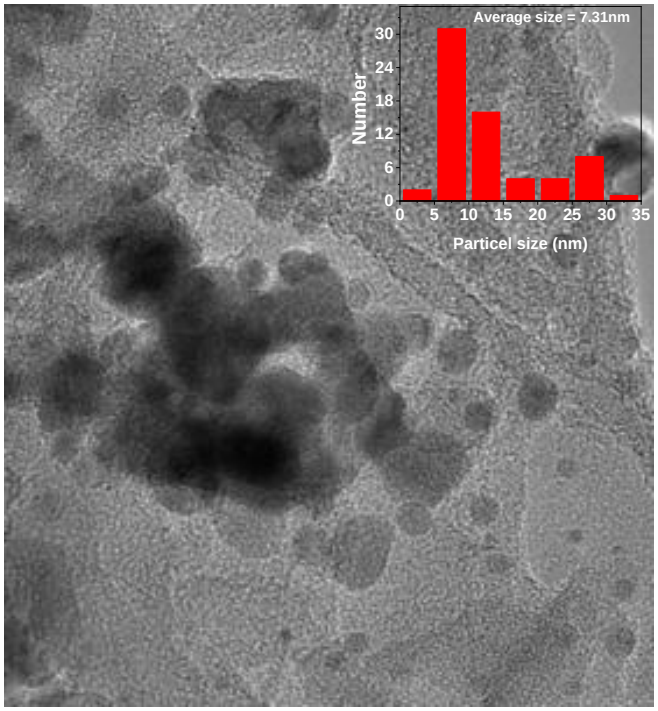

Figure S4. Transmission Electron Microscopy image of PdO/C_3N_4

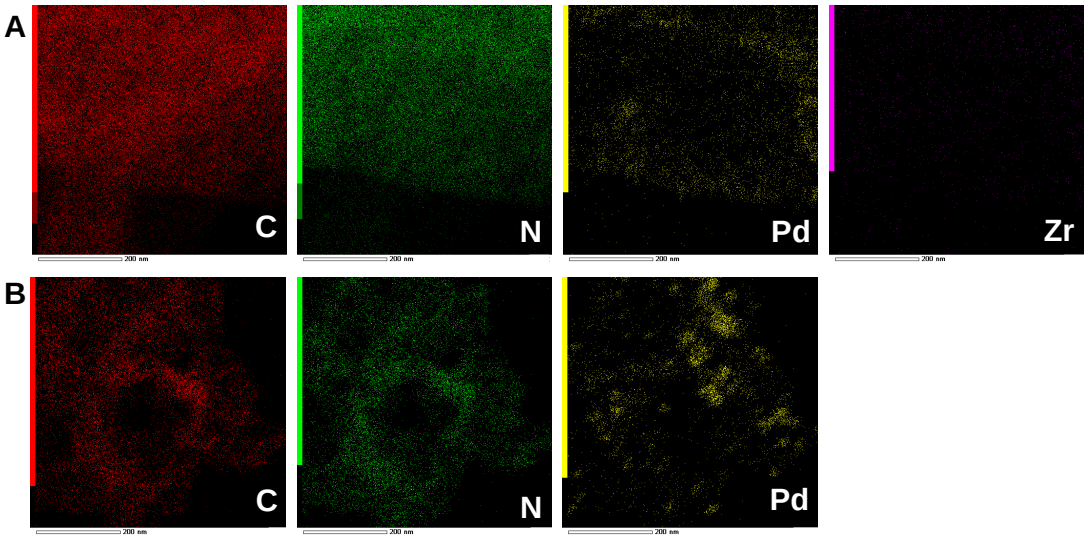

Figure S5. Elemental mapping of (A) $PdO/Zr\text{-}C_3N_4$ and (B) PdO/C_3N_4.

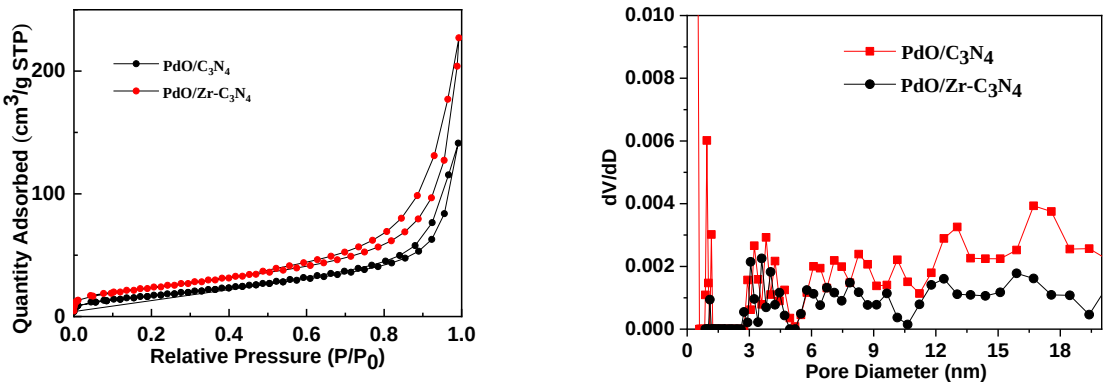

Figure S6. N_2 adsorption/desorption isotherm at 77 K and pore size distribution curve for the PdO/Zr-C_3N_4.

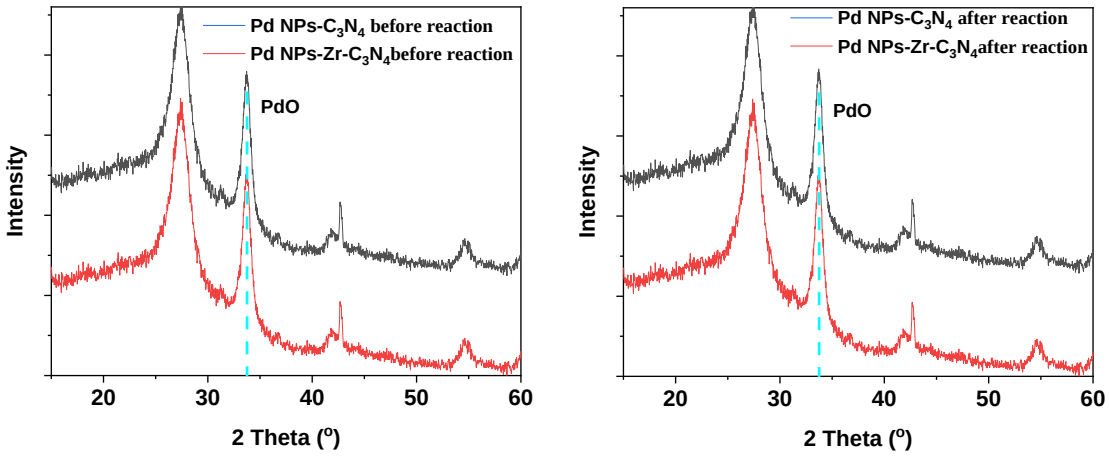

Figure S7. Powder X-ray diffraction patterns (XRD) patterns of PdO NPs/Zr-C_3N_4 and PdO NPs/C_3N_4 catalysts.

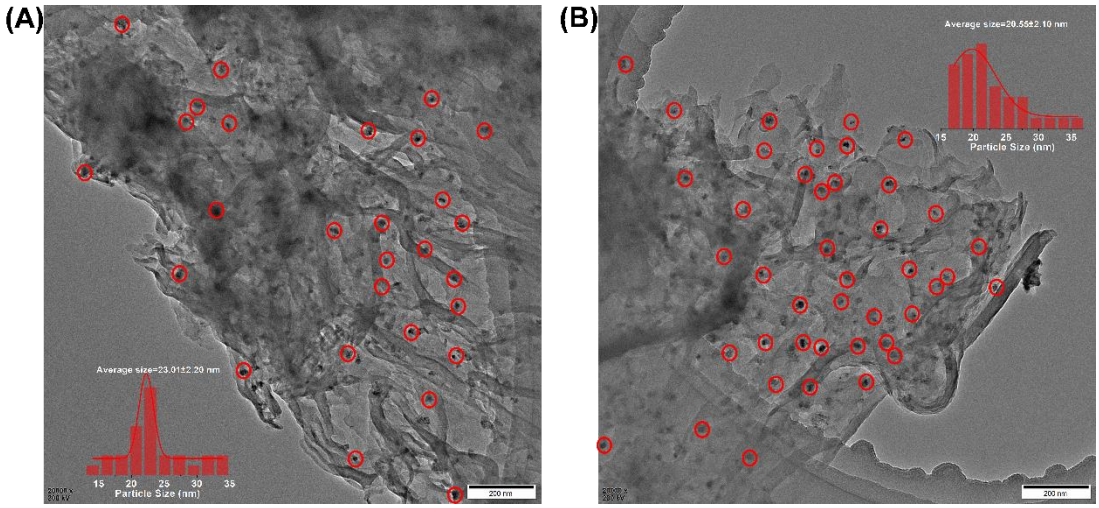

Figure S8. Transmission Electron Microscopy image of (A) PdO NPs/C_3N_4 and (B) PdO NPs/Zr-C_3N_4.

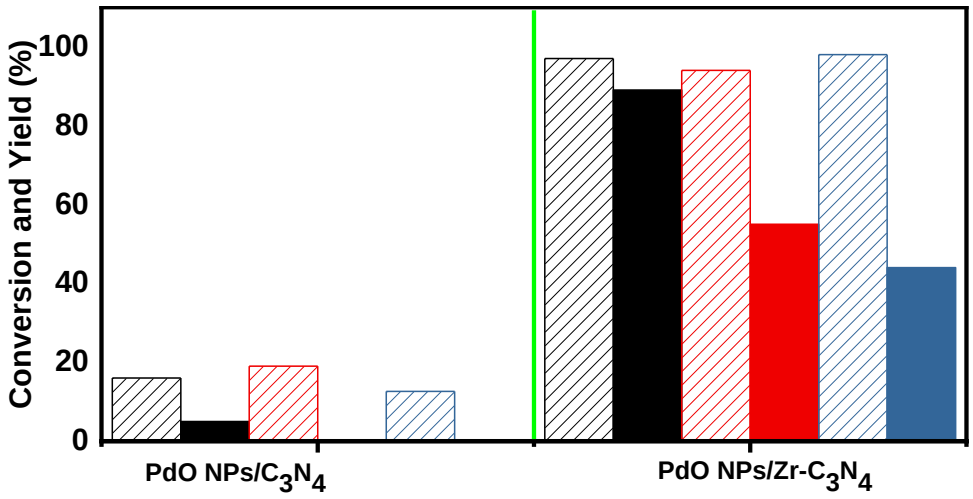

Figure S9. Catalytic dehydrogenation of H-LOHCs over (A) PdO NPs supported on C_3N_4 and Zr-C_3N_4. Reaction conditions: 250 mg HR-LOHCs, 125 mg catalyst, 140 °C of reaction temperature and 8 h of reaction time.

As shown by the XRD in Figure S7, both the PdO NPs/Zr-C_3N_4 and PdO NPs/C_3N_4 catalysts exhibited at $2\theta = 27.2^{o}$ [corresponding to the typical (100) and (002) planes for g-C_3N_4], and 33.9, 41.9 and 54.7° [corresponding to the (101), (111) and (112) planes for PdO], respectively. The intensity and full width at half maximum (FWHM) of the PdO NPs was almost the same, indicating that the PdO NPs are dispersed almost the same on the Zr-C_3N_4 and C_3N_4. The TEM results as shown in the Figure S8 also prove this conclusion and the

average particle size for the PdO in PdO NPs/Zr-C_3N_4 and PdO NPs/C_3N_4 was 20.55±2.1 nm and 23.01±2.2 nm. At the reaction temperature of 140 °C for 8 h, lower than 20% conversion of each component (12H-NECZ, 8H-MID and 12H-NPCZ) was obtained over the selected PdO NPs/C_3N_4 and only 5% yield of MID was obtained (Figure S9). However, for the PdO NPs/Zr-C_3N_4, the conversion of the 12H-NECZ, 8H-MID and 12H-NPCZ reached 97%, 94%, and 98%, and the yields of the completely dehydrogenated products (NECZ, MID and NPCZ) was 89%, 55% and 46%, respectively, which showed significantly enhanced performance than that of the PdO NPs/C_3N_4 catalysts under the otherwise same reaction conditions and the same PdO particle size.

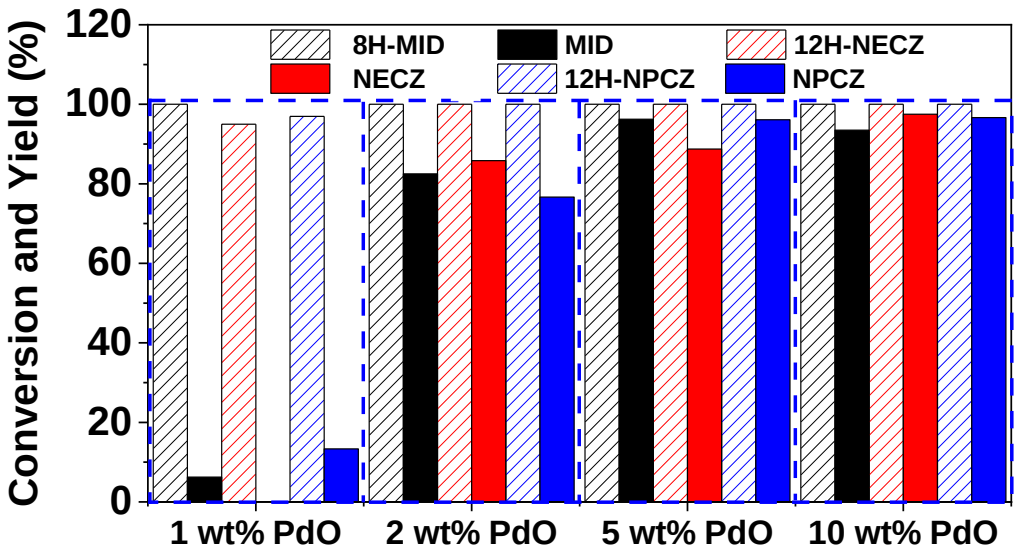

Figure S10. Catalytic dehydrogenation of H-LOHCs over PdO supported on Zr-C_3N_4 with different PdO loading. Reaction conditions: 250 mg HR-LOHCs, 125 mg catalyst, 140 °C of reaction temperature and 8 h of reaction time.

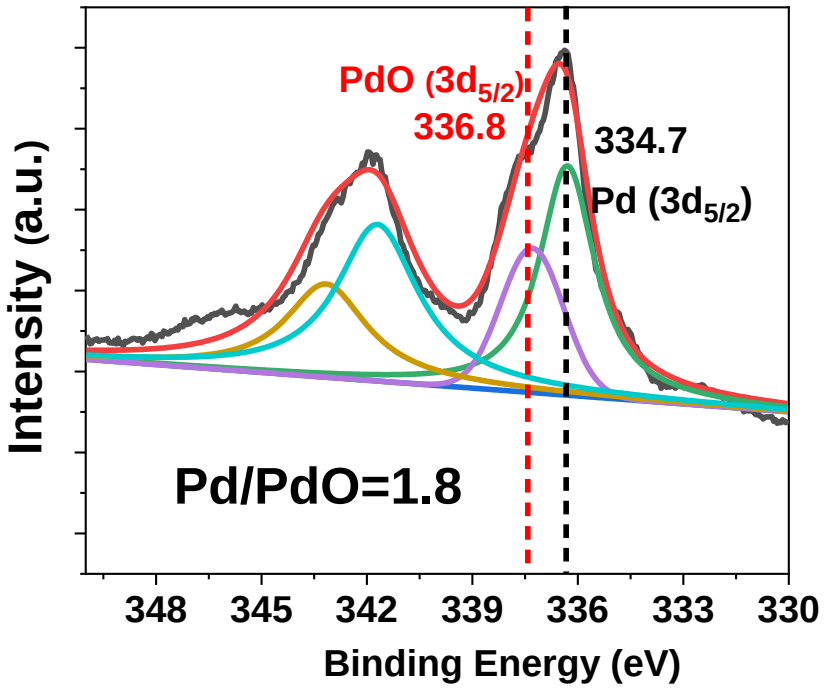

Figure S11 X-ray photoelectron spectroscopy (XPS) of Pd/Zr-C_3N_4 after oxidized with 2h under the same procedure

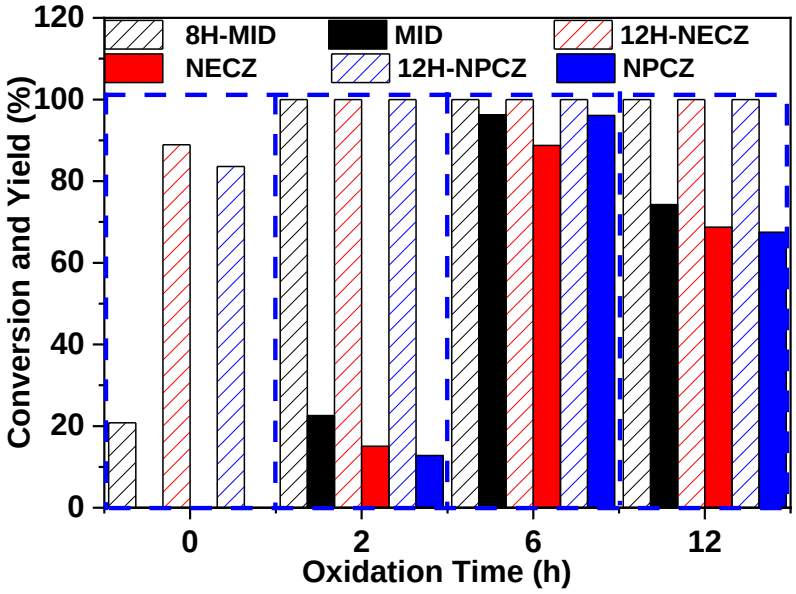

Figure S12. Catalytic dehydrogenation of H-LOHCs over PdO supported on Zr-C_3N_4 with different oxidation time. Reaction conditions: 250 mg HR-LOHCs, 125 mg catalyst, 140 °C of reaction temperature and 8 h of reaction time.

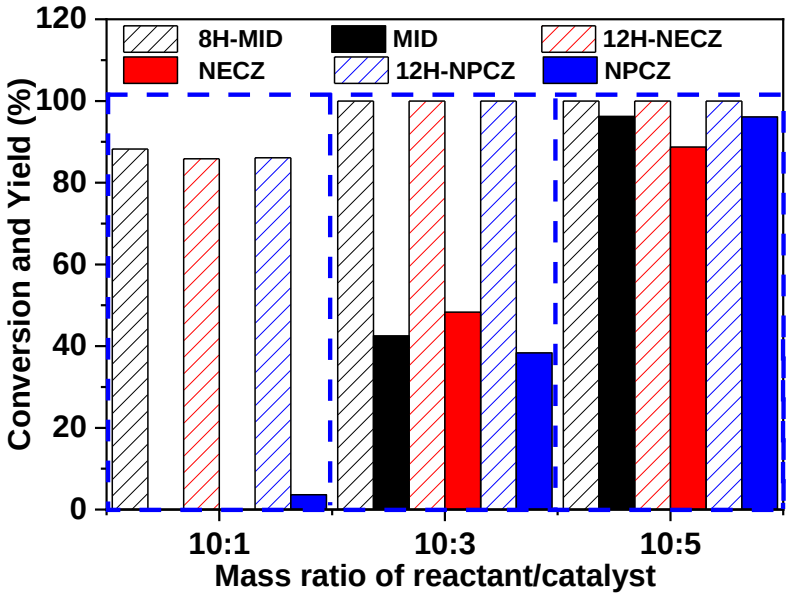

Figure S13. Catalytic dehydrogenation of H-LOHCs over PdO supported on Zr-C_3N_4 with different mass ratio of reactant/catalyst. Reaction conditions: 250 mg HR-LOHCs, 125 mg catalyst, 140 °C of reaction temperature and 8 h of reaction time.

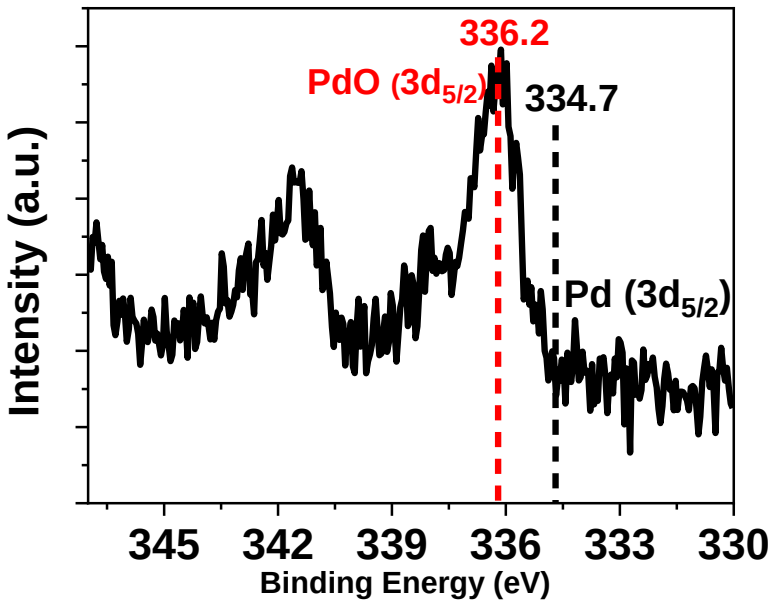

Figure S14. X-ray photoelectron spectroscopy (XPS) of PdO/Zr-C_3N_4 after reaction of 8h under 140 °C.

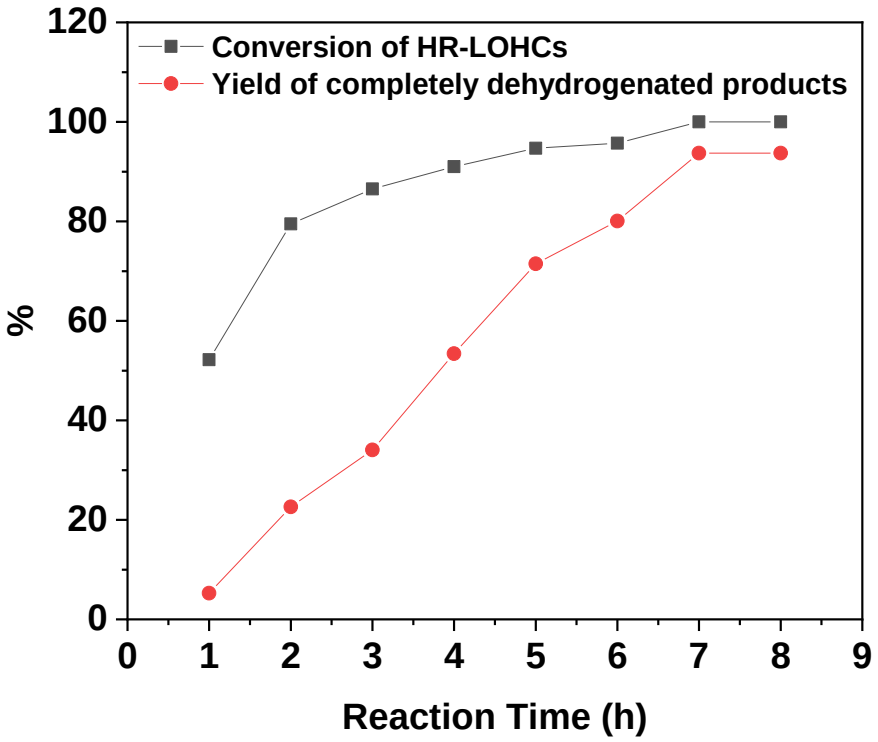

Figure S15. Catalytic dehydrogenation of H-LOHCs over PdO supported on Zr-C_3N_4 with different reaction time. Reaction conditions: 250 mg HR-LOHCs, 125 mg catalyst, 140 °C of reaction temperature and 0-8 h of reaction time.

Table S1 Textural properties of series serious PdO supported catalysts.

Samples	S_{BET} (m^2/g)	V_{meso} (m^2/g)	V_{total} (cm^3/g)	V_{meso} (cm^3/g)
PdO/C_3N_4	56.90	56.90	0.21	0.21
PdO/Zr-C_3N_4	79.66	79.66	0.33	0.33

Table S2. The catalytic activity of the catalysts reported for dehydrogenation

N-heteromatics	Dehydrogenation product	Selected dehydrogenation catalyst	Temperature /°C	Ref
12H-NECZ	NECZ	Pd/Al_2O_3	180	[4, 10-11]
12H-NECZ	NECZ	$PdRu/Al_2O_3$	180	[12]
12H-NECZ	NECZ	$PdCr/Al_2O_3$	195	[13]
12H-NECZ	NECZ	$Pt@\gamma\text{-}Al_2O_3$ /α- Al_2O_3	235	[14]
12H-NECZ	NECZ	$PdPt/TiO_2$	195	[15]
12H-NECZ	NECZ	Pt/TiO_2	180	[16-17]
12H-NECZ	NECZ	$Au_1Pd_{1.3}/rGO$	180	[18]

12H-NECZ	NECZ	Pd/rGO	180	[19]
12H-NECZ	NECZ	$Pd_{1.2}Cu$/rGO	180	[3]
12H-NECZ	NECZ	Pd/CNT	260	[20]
12H-NECZ	NECZ	$PdAu/SiO_2$	180	[21]
12H-NECZ	NECZ	$Co\text{-}B/Al_2O_3\text{-}YH_{3-x}$	200	[22]
8H-MID	MID	Pd/Al_2O_3	170	[23]

Table S3. CO uptake and calculated TOF of $PdO/Zr\text{-}C_3N_4$ and PdO/C_3N_4.

	CO uptake μmol/g	TOF h^{-1}
$PdO/Zr\text{-}C_3N_4$	54.81	2421.58
PdO/C_3N_4	17.10	842.92

References

1. Lin, W.; Yao, S.; Chen, H.; Li, S.; Xia, Y.; Yao, Y.; Li, J.; Cheng, D.; Fu, J., A new trick on an old support: Zr in situ defects-created carbon nitride for efficient electrochemical nitrogen fixation. *J. Energy Chem.* **2021,** *53*, 109-115.
2. Mazumder, V.; Sun, S., Oleylamine-mediated synthesis of Pd nanoparticles for catalytic formic acid oxidation. *J.Am. Chem. Soc.* **2009,** *131* (13), 4588-4589.
3. Wang, B.; Chang, T.-y.; Jiang, Z.; Wei, J.-j.; Fang, T., Component controlled synthesis of bimetallic PdCu nanoparticles supported on reduced graphene oxide for dehydrogenation of dodecahydro-N-ethylcarbazole. *Appl. Catal. B: Environ.* **2019,** *251*, 261-272.
4. Dong, Y.; Yang, M.; Mei, P.; Li, C.; Li, L., Dehydrogenation kinetics study of perhydro-N-ethylcarbazole over a supported Pd catalyst for hydrogen storage application. *Int. J. Hydrogen. Energy* **2016,** *41* (20), 8498-8505.
5. Eblagon, K. M.; Tam, K.; Yu, K.; Tsang, S., Comparative study of catalytic hydrogenation of 9-ethylcarbazole for hydrogen storage over noble metal surfaces. *J. Phys. Chem. C* **2012,** *116* (13), 7421-7429.
6. Eblagon, K. M.; Tam, K.; Tsang, S. C. E., Comparison of catalytic performance of supported ruthenium and rhodium for hydrogenation of 9-ethylcarbazole for hydrogen storage applications. *Energy Environ. Sci.* **2012,** *5* (9), 8621-8630.
7. Dong, Y.; Yang, M.; Yang, Z.; Ke, H.; Cheng, H., Catalytic hydrogenation and dehydrogenation of N-ethylindole as a new heteroaromatic liquid organic hydrogen carrier. *Int. J. Hydrogen. Energy* **2015,**

40 (34), 10918-10922.

8. Yang, M.; Dong, Y.; Fei, S.; Pan, Q.; Ni, G.; Han, C.; Ke, H.; Fang, Q.; Cheng, H., Hydrogenation of N-propylcarbazole over supported ruthenium as a new prototype of liquid organic hydrogen carriers (LOHC). *RSC Adv.* **2013,** *3* (47), 24877-24881.

9. Sotoodeh, F.; Smith, K. J., Kinetics of hydrogen uptake and release from heteroaromatic compounds for hydrogen storage. *Ind. Eng. Chem. Res.* **2010,** *49* (3), 1018-1026.

10. Yang, M.; Dong, Y.; Fei, S.; Ke, H.; Cheng, H., A comparative study of catalytic dehydrogenation of perhydro-N-ethylcarbazole over noble metal catalysts. *Int. J. Hydrogen. Energy* **2014,** *39* (33), 18976-18983.

11. Peters, W.; Eypasch, M.; Frank, T.; Schwerdtfeger, J.; Körner, C.; Bösmann, A.; Wasserscheid, P., Efficient hydrogen release from perhydro-N-ethylcarbazole using catalyst-coated metallic structures produced by selective electron beam melting. *Energy Environ. Sci.* **2015,** *8* (2), 641-649.

12. Zhu, T.; Yang, M.; Chen, X.; Dong, Y.; Zhang, Z.; Cheng, H., A highly active bifunctional Ru–Pd catalyst for hydrogenation and dehydrogenation of liquid organic hydrogen carriers. *J. Catal.* **2019,** *378*, 382-391.

13. Tarasov, A. L.; Tkachenko, O. P.; Kustov, L. M., Mono and Bimetallic Pt–(M)/Al 2 O 3 Catalysts for Dehydrogenation of Perhydro-N-ethylcarbazole as the Second Stage of Hydrogen Storage. *Catal. Lett.* **2018,** *148* (5), 1472-1477.

14. Peters, W.; Seidel, A.; Herzog, S.; Bösmann, A.; Schwieger, W.; Wasserscheid, P., Macrokinetic effects in perhydro-N-ethylcarbazole dehydrogenation and H 2 productivity optimization by using egg-shell catalysts. *Energy Environ. Sci.* **2015,** *8* (10), 3013-3021.

15. Kustov, L.; Tarasov, A.; Kirichenko, O., Microwave-activated dehydrogenation of perhydro-N-ethylcarbazol over bimetallic Pd-M/TiO2 catalysts as the second stage of hydrogen storage in liquid substrates. *Int. J. Hydrogen. Energy* **2017,** *42* (43), 26723-26729.

16. Jiang, Z.; Gong, X.; Wang, B.; Wu, Z.; Fang, T., A experimental study on the dehydrogenation performance of dodecahydro-N-ethylcarbazole on M/TiO2 catalysts. *Int. J. Hydrogen. Energy* **2019,** *44* (5), 2951-2959.

17. Gong, X.; Jiang, Z.; Fang, T., Enhancing selectivity and reducing cost for dehydrogenation of dodecahydro-N-ethylcarbazole by supporting platinum on titanium dioxide. *Int. J. Hydrogen. Energy* **2020,** *45* (11), 6838-6847.

18. Wang, B.; Chang, T.-y.; Gong, X.; Jiang, Z.; Yang, S.; Chen, Y.-s.; Fang, T., One-pot synthesis of Au/Pd core/shell nanoparticles supported on reduced graphene oxide with enhanced dehydrogenation performance for dodecahydro-N-ethylcarbazole. *ACS Sustainable Chem. Eng.* **2018,** *7* (1), 1760-1768.

19. Wang, B.; Yan, T.; Chang, T.; Wei, J.; Zhou, Q.; Yang, S.; Fang, T., Palladium supported on reduced graphene oxide as a high-performance catalyst for the dehydrogenation of dodecahydro-N-ethylcarbazole. *Carbon* **2017,** *122*, 9-18.

20. Zhu, M.; Xu, L.; Du, L.; An, Y.; Wan, C., Palladium supported on carbon nanotubes as a high-performance catalyst for the dehydrogenation of dodecahydro-N-ethylcarbazole. *Catalysts* **2018,** *8* (12), 638.

21. Jiang, Z.; Guo, S.; Fang, T., Enhancing the Catalytic Activity and Selectivity of PdAu/SiO2 Bimetallic Catalysts for Dodecahydro-N-ethylcarbazole Dehydrogenation by Controlling the Particle Size and Dispersion. *ACS Applied Energy Materials* **2019,** *2* (10), 7233-7243.

22. Wu, Y.; Guo, Y.; Yu, H.; Jiang, X.; Zhang, Y.; Qi, Y.; Fu, K.; Xie, L.; Li, G.; Zheng, J., Nonstoichiometric Yttrium Hydride–Promoted Reversible Hydrogen Storage in a Liquid Organic

Hydrogen Carrier. *CCS Chem.* **2020**, 974-984.
23. Yang, M.; Cheng, G.; Xie, D.; Zhu, T.; Dong, Y.; Ke, H.; Cheng, H., Study of hydrogenation and dehydrogenation of 1-methylindole for reversible onboard hydrogen storage application. *Int. J. Hydrogen. Energy* **2018,** *43* (18), 8868-8876.